POLITECNICO DI TORINO
Repository ISTITUZIONALE

Reliability assessment of concrete walls as rockfall protection systems in mountainous areas

Original
Reliability assessment of concrete walls as rockfall protection systems in mountainous areas / Marchelli, M., De Biagi, V.. - (2026), pp. 243-250. (EURO-C 2026: Computational Modelling of Concrete and Concrete Structures Seefeld (Aut) 9-12 marzo 2026) [10.1201/9781003660026-28].

Availability:
This version is available at: 11583/3008537 since: 2026-03-10T16:16:51Z

Publisher:
CRC Press

Published
DOI:10.1201/9781003660026-28

Terms of use:

This article is made available under terms and conditions as specified in the corresponding bibliographic description in the repository

Publisher copyright

(Article begins on next page)

15 November 2026

Computational Modelling of Concrete and Concrete Structures – Meschke, Pichler & Rots (Eds)
© 2026 The Author(s), ISBN: 978-1-041-11408-6

Reliability assessment of concrete walls as systems for low impacted energies in steep mountainous areas

M. Marchelli
Department of Environment, Land and Infrastructure Engineering, Politecnico di Torino, Torino, Italy

V. De Biagi
Department of Structural, Geotechnical and Building Engineering, Politecnico di Torino, Torino, Italy

ABSTRACT: Rockfall protection systems are essential for safeguarding infrastructure and human activities in mountainous regions, where falling rock masses pose persistent hazards that can cause severe damages. Structural mitigation measures, such as energy-dissipating barriers, are commonly installed near roads, buildings, and industrial facilities to reduce impact forces. These systems function by either absorbing the kinetic energy of falling blocks through deformation or resisting impact via mass and frictional dissipation. Two main energy dissipation strategies characterize these systems. Flexible barriers, such as net fences, absorb energy through large deformations and are widely used for their adaptability and effectiveness across varying block sizes. However, they require sufficient clearance between the barrier and protected infrastructure, which limits their application in narrow corridors. To overcome this constraint, rigid systems, such as L-shaped reinforced concrete walls, have been developed. For high-impact energies, a cushion layer of granular material is often added to the upslope face of the wall. However, this solution requires a large footprint, which is not always feasible, and in steep areas, the added weight can even lead to overall slope instability. Therefore, for expected impact energies up to approximately 800 kJ, a rigid system alone can represent an effective and economical solution. These structures rely on mass and bending resistance to dissipate energy without requiring buffer space, making them suitable for constrained environments. Nevertheless, their long-term reliability under diverse impact conditions remains an open question. This study introduces a time-integrated reliability analysis of rigid rockfall protection systems, focusing on performance under variable loading over extended periods. The approach incorporates the frequency–magnitude distribution of rockfall events, acknowledging that smaller blocks occur more frequently than larger ones. Variability in block mass, impact velocity, and kinetic energy is modelled within a probabilistic framework that accounts for uncertainties in material properties and structural response. The analysis is applied to a real-world slope with documented rockfall activity, evaluating the reliability of a concrete wall system under cumulative low-energy impacts and rare high-energy events. Using limit state functions, failure probabilities and critical performance thresholds are estimated. Results emphasize the importance of integrating temporal and probabilistic dimensions into design, showing that rigid barriers, while effective in constrained spaces, exhibit reliability sensitivity to impact frequency, energy dissipation capacity, and degradation over time.

1 INTRODUCTION

Rockfalls are highly energetic gravitational phenomena characterised by the detachment and downslope movement of single or aggregated rock masses (Hungr et al. 2014). These events represent one of the most hazardous processes in mountainous regions, posing significant risks to infrastructure, transportation corridors, and human safety. Their occurrence is often triggered by natural factors such as weathering, freeze-thaw cycles, seismic activity, or intense rainfall, which reduce slope stability and promote block detachment (Delonca et al. 2014). The motion of released blocks typically occurs in successive phases, alternating between free-fall through the air and interactions with the slope surface. Each impact modifies the block's trajectory and dissipates part of its kinetic energy, while the type of motion, e.g. rolling, sliding, or bouncing, depends on slope geometry, surface roughness, and soil conditions. The path traced by a reference point on the falling block is referred to as its trajectory (Li and Lan 2015). Predicting rockfall trajectories is inherently challenging due to the randomness of block-slope interactions and the uncertainties associated with natural processes. Variability in block shape, size, and material

DOI: 10.1201/9781003660026-28
This chapter has been made available under a Creative Commons [Attribution-Non Commercial-No Derivatives (CC-BY-NC-ND)] 4.0 license



Figure 1. Photo of a rockfall event occurred in Cogne, Italy, on 16 September 2016 after heavy rains. Source: Catasto Dissesti RAVA, F-16-09-2016-00-v-Cm-x.

properties, combined with heterogeneous slope conditions, introduces stochastic behaviour that cannot be captured by deterministic models alone. For this reason, modern rockfall propagation analyses rely on physics-based models coupled with probabilistic approaches, where input parameters are sampled from probability distributions to generate a set of possible trajectories (Leine et al. 2014).

The occurrence of rockfalls can cause severe damage, particularly when such phenomena affect highly urbanized areas. While human settlements have traditionally been established in relatively safe zones, transportation infrastructures, such as roads and railways, often traverse regions exposed to rockfall hazards. This spatial overlap between critical infrastructure and unstable slopes significantly increases the potential for accidents, service disruptions, and economic losses. When a rock block interacts with a roadway, several outcomes are possible: the block may collide with a vehicle, stop on the way, or damage the pavement, compromising driver safety and traffic continuity. Figure 1 shows a 0.5 m^3 block stopped on the road after a rockfall event. Since rockfall triggering factors are strongly influenced by weather conditions, climate change is expected to increase both the frequency and severity of these events, potentially affecting previously safe settlements as well. According to the U.S. Geological Survey (USGS), landslides, including rockfalls, cause approximately 25 to 50 fatalities annually worldwide. Rockfalls are also among the leading causes of death in specific high-risk environments, such as high-altitude mountaineering, where an average of 22.2 fatalities per year have been reported in the Swiss Alps by Benedikt (2024), coastal environment and in quarry operations. Furthermore, Corominas and colleagues compiled a historical catalogue of rockfalls in Spain, documenting 1,118 events over more than two centuries, which resulted in 1,550 deaths and approximately 2,184 injuries with a distinct increase in the last 20 years especially on road infrastructures (Corominas et al. 2025).

Rockfall risk mitigation can be achieved through different techniques, depending on factors such as the type of mass, slope characteristics, extent of the phenomenon, and other constraints, such as accessibility of specific areas and associated costs (Maheshwari et al. 2023). Slopes can be engineered by means of preventive or protective mitigation measures. Preventive measures aim to stabilise the slope itself and prevent rock detachment by bolting or anchoring individual blocks, or by installing mesh and drapery systems. These solutions are generally feasible when the number of potentially unstable blocks is limited and their positions are well identified. Although bolts combined with meshes effectively reduce risk, their application becomes economically unfeasible when the release area is extensive. Protective mitigation measures, on the other hand, consist of systems designed to intercept and arrest falling rock masses. Their design derives from the outputs of the trajectory analysis, which provides the heights and the velocity of the blocks the the site of the measure as probability distributions. These solutions are installed near the element to be protected and can stop blocks with energies up to several hundred megajoules. They are typically grouped into three categories: (i) rockfall sheds or tunnels, which are reinforced concrete structures with a buffer layer of soil or other material on top to absorb impact energy; (ii) rockfall embankments, which are geotechnical structures composed of compacted soil layers that dissipate kinetic energy through their large mass; and (iii) net fences or flexible barriers, which are lightweight steel structures equipped with engineered components, such as net and brakes, that dissipate the energy of impacting blocks. These systems can arrest blocks with energies up to 12.5 MJ, equivalent to the kinetic energy of a 26-ton block travelling at 30 m/s (approximately 108 km/h). The deceleration imposed by the barrier results in large displacements, which can reach up to 8 meters.

Although flexible barriers are widely used due to their adaptability and effectiveness in intercepting a range of block sizes, their performance depends on the availability of sufficient working space between the system and the protected infrastructure. Barriers installed along roads can effectively stop falling rocks; however, their deformation may pose a risk to road users by encroaching into the traffic lane. This spatial requirement represents a significant limitation, particularly in narrow corridors or near roadways. To overcome this constraint, rigid protection systems, such as L-shaped reinforced concrete walls, have been developed. If the upslope space is enough and the slope overall stability is not compromised a cushion layer can be designed to absorb some of the impacting energy and redistribute the stresses on the wall. Nevertheless, in steep mountain areas with narrow roads, this kind of systems is not achievable and a L-shape

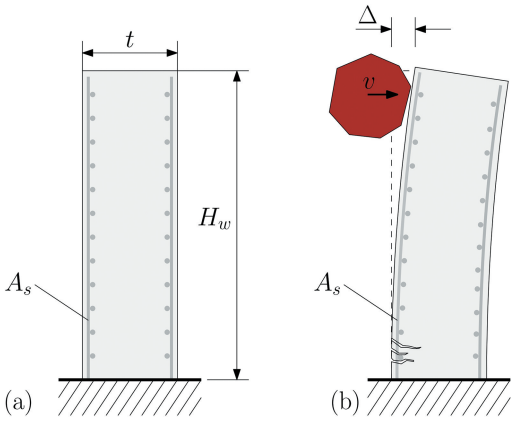


Figure 2. Sketch of the concrete wall to protect the road infrastructure from falling rocks: (a) geometry, (b) the maximum displacement during impact.

reinforced concrete wall alone can represent a profitable solution when the expected impacted energies are limited. These structures rely on their substantial mass and capacity to resist the momentum of falling blocks, dissipating energy through bending deformation and friction during impact, without requiring a buffer zone. While these systems offer clear spatial advantages, their long-term reliability under varying impact conditions remains an open question. The present paper introduces a reliability-based assessment of the safety of such protective measures, providing an estimate of the probability of failure, a key metric for quantifying residual risk.

2 IMPACT OF A BLOCK AGAINST A CANTILEVER WALL

Let us consider a concrete wall vertically installed close to the element at risk, say the road, as depicted in Figure 2.a. The wall has a height H_w and a thickness t. For sake of simplicity, wall is considered long enough to protect the entire portion of road affected by the phenomenon. The wall has reinforcement bars in the upslope side to resist the bending generated by the impacting block. Considering the upslope reinforcement, the vertical reinforcement ratio $q = A_s/t$ is defined, where A_s is the area of vertical reinforcement along one metre of wall. The classical RC properties are introduced: f_c and E_c are compressive strength and Young's modulus of concrete, f_y and E_s are yield strength and Young's modulus of steel, respectively. The density of the concrete, ρ_c, is set at 2500 kg/m^3. The impacting block exerts a force on the cantilever, whose direction depends on the trajectory and is rarely perfectly horizontal. For simplicity, the impact is assumed to occur horizontally, as shown in Figure 2b. Using well-established structural

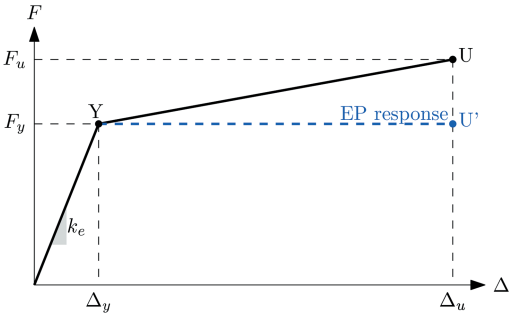


Figure 3. Sketch of the response curve.

engineering approaches, the compliance curve of the wall subjected to a horizontal force at the impact height, H_i, can be derived. Starting from the moment-curvature relationship of a concrete cross-section, idealised as a bilinear curve, the expected bilinear force-displacement response is shown in Figure 3. Up to the yielding point (Y), corresponding to the onset of plasticity at the base of the cantilever, the response is elastic and characterised by an effective stiffness k_e, which relates the displacement Δ to the applied horizontal force at H_i. After yielding, a plastic hinge forms, resulting in a limited hardening phase, as the system is statically determinate and offers no plastic reserve beyond the cross-section level. The ultimate point (U) defines the system's final capacity, with a force F_u similar to the yielding force but associated with a larger displacement Δ_u, reflecting the system's ductility. The area under the curve represents the strain energy stored in the system. An elastic–plastic response, illustrated by the dashed blue curve in Figure 3, neglects hardening in the post-yield phase, providing a conservative estimate of the energy.

A mass m with a velocity v colliding against a wall of mass M transfers its momentum to the impactor in such a way the velocity of mass and target are the same. When dealing with a body different from a point mass, the mass participating to the motion, namely the generalised mass, may not be the total mass of the body. In an elastic cantilever subjected to an impact at the free end, the generalised mass, M_g^e, is $33/140 \approx 1/4$ of the total mass M, i.e., $M_g^e = 1/4M$. On the contrary, when the cantilever enters in the plastic stage, the generalised mass, M_g^p, is 1/3 of the total mass, i.e., $M_g^p = 1/3M$. In the present analysis, the coefficient of restitution of the impacting mass is equal to zero. This hypothesis holds as the impacted system is deformable and, hence, the wall deforms during the collision up to the maximum displacement. In the recovery phase, the block is subjected to a restitution. This hypothesis is conservative as it considers that all the energy of the impacting block is transferred to the wall. Similarly, a strip of wall of width equal to three times the impacting block diameter, ϕ, is considered,

i.e., $M = 3tH_w\phi\rho$. When the two masses enter in contact, for momentum conservation, their velocity, v_0, is equal to:

$$v_0 = \frac{m}{m + M_g^e} v. \tag{1}$$

The resulting kinetic energy, K_0, is equal to:

$$K_0 = \frac{1}{2}\left(m + M_g^e\right) v_0^2 = \frac{1}{2}\frac{m}{m + M_g^e} mv^2. \tag{2}$$

The resulting kinetic energy is dissipated in the system as strain energy up to the maximum displacement, resulting in the maximum forces in the system. The following vibration regime is not investigated here. Similarly, concrete damping is not considered, as well, for the impulsive nature of the phenomenon.

Depending on K_0, the system undergoes elastic or elasto-plastic displacements. Case 1 refers to situations for which $K_0 \leq S_y$, being S_y the strain energy associated to yielding, i.e., $S_y = 1/2 k_e \Delta_y^2$, that correspond to an elastic behavior of the wall. Case 2, for which $K_0 > S_y$ relates to plastic-dissipation.

2.1 *Case 1: elastic response, $K_0 \leq S_y$*

If the kinetic energy K_0 is smaller than the maximum elastic energy that can be stored in the system S_y, the maximum displacement is smaller than Δ_y. The kinetic energy is converted in strain energy and the following equality holds:

$$\frac{1}{2}\frac{m}{m + M_g^e} mv^2 = \frac{1}{2} k_e \Delta^2, \tag{3}$$

from which it results:

$$\Delta = v\sqrt{\left(\frac{m}{k_e}\right)\left(\frac{m}{m + M_g^e}\right)}. \tag{4}$$

The system that lies in the elastic stage resists the impact.

2.2 *Case 2: elastic-plastic response, $K_0 > S_y$*

In this case, the total kinetic energy can be partitioned as:

$$K_0 = S_y + S_p, \tag{5}$$

where S_p is the plastic strain energy. At the end of the elastic phase, when the system reaches a displacement Δ_y, the residual kinetic energy is equal to:

$$K_0 - S_y = \frac{1}{2}\left(\frac{m}{m + M_g^e} mv^2 - k_e \Delta_y^2\right), \tag{6}$$

resulting in a velocity v_y equal to:

$$v_y = \sqrt{\left(\frac{m}{m + M_g^e}\right)^2 v^2 - \left(\frac{k_e}{m + M_g^e}\right)\Delta_y^2}, \tag{7}$$

Being the generalized mass in the plastic phase, M_g^p, different from the previous one, momentum conservation provides the velocity, v_p, of the system of masses at the onset of plasticity, as:

$$v_p = \frac{m + M_g^e}{m + M_g^p} v_y, \tag{8}$$

with a resulting kinetic energy K_p equal to:

$$K_p = \frac{1}{2}\frac{\left(m + M_g^e\right)^2}{m + M_g^p}\left[\left(\frac{m}{m + M_g^e}\right)^2 v^2 + - \left(\frac{k_e}{m + M_g^e}\right)\Delta_y^2\right]. \tag{9}$$

The kinetic energy is then dissipated through permanent deformation, resulting in a total displacement equal to:

$$\Delta = \Delta_y + \frac{K_p}{k_e \Delta_y}. \tag{10}$$

If $\Delta \leq \Delta_u$ the system resists the impact. If the inequality does not hold, the protective wall fails.

3 INCLUDING ROCKFALL VARIABILITY INTO THE CALCULATIONS

Rockfall is an extremely variable phenomenon. As previously shown, the trajectories can vary due to the topography and the randomness in the interaction between block and slope. In addition, the size of the released mass largely varies. Studies indicate that smaller rock volumes are more prone to detachment than larger blocks. Research on in-situ block size distributions suggests that rock mass discontinuities

identify potentially unstable blocks, with volumes following an exponential-like distribution (Moos et al. 2022). De Biagi et al. (2017) formulated a relationship between released block volumes and their return period. The effects of the interaction with the protective wall should include such variability. Recently, the Authors have formulated a time independent reliability-based framework for rockfall net fences, which is at the base of the methodology here described (De Biagi et al. 2020, Marchelli et al. 2021, Marchelli et al. 2020). In their approach, the occurrence process is described through a Poisson distribution, while the distribution of the fallen masses follow a Pareto distribution.

The failure probability of the protective RC wall is the result of two failure scenarios: (i) a failure due to the inability of the system to intercept the blocks since it is not enough tall, to which a probability p_h is associated, (ii) a failure due to the inability of the system to arrest the intercepted blocks since it is not enough strong, p_k. The total failure probability, p, is the sum of the two terms:

$$p = p_h + p_k. \tag{11}$$

Each failure mode is described through a state function. The state function related to the excessive height, S_h, is expressed as a function of the trajectory height, h, and diameter of the block, ϕ, depending upon the mass:

$$S_h = H_w - h - \frac{\phi}{2}. \tag{12}$$

The state function related to the excessive kinetic energy is expressed as a function of expected displacements at the free end of the wall as:

$$S_k = \Delta_u - \Delta, \tag{13}$$

where Δ is a function of velocity and mass of the impacting block, as described in Section 2. Following the approach described in the previous works of the Authors, it results:

$$p_h = 1 - \exp\left\{-\lambda\tau\left[\int_0^\infty p_{fh}|(m_k = \mu) f_m(\mu) d\mu\right]\right\}, \tag{14}$$

with λ the annual mean frequency of rockfall events reaching the protection and τ the duration of the reference period during which the risk is computed, namely 1 year. The term $f_m(\mu)$ is the probability of having during the certain occurrence of an event a mass equal to μ, derived from the Pareto distribution. Finally, the term $p_{fh}|(m_k = \mu)$ is the failure probability due to excessive height if the mass has value equal to μ, and it is computed as:

$$p_{fh}|(m_k = \mu) = \iiint_{S_h \le 0} f_H(m_k = \mu) dH_w dh dm, \tag{15}$$

where $f_H(m_k = \mu)$ is the joint probability density function of the mass (with characteristic value equal to μ), the height of the impacting bloc and the nominal height of the wall.

In a similar manner, the failure related to excessive kinetic energy can be written as:

$$p_k = 1 - \exp\left\{-\lambda\tau\left[\int_0^\infty p_{fk}|(m_k = \mu) f_m(\mu) d\mu\right]\right\}. \tag{16}$$

Table 1. Results of the trajectory analyses.

	Height	Velocity
95th percentile	3.02 m	14.0 m/s
99th percentile	3.75 m	14.7 m/s

The term $p_{fk}|(m_k = \mu)$ is the failure probability due to excessive kinetic energy if the mass has value equal to μ, and it is computed as:

$$p_{fk}|(m_k = \mu) = \iiint_{S_k \le 0} f_K(m_k = \mu) d\Delta_u dm dv, \tag{17}$$

where $f_K(m_k = \mu)$ is the joint probability density function of the mass (with characteristic value equal to μ), the ultimate displacement of the wall, and the velocity of the block.

4 EXAMPLE

The proposed solution is adopted to protect a mountain road from rockfall events. From a geotechnical point of view, the site is characterised by a moderate activity. The database of previous events highlight an average frequency of events larger than 0.2 m^3, i.e. 540 kg mass, of about 1 event every 10 years ($\lambda = 0.1$). The distribution of the already fallen masses in the proximity of the road shows a large-to-small volumes ratio with a moderate differentiation, with a Pareto Type 1 shape distribution coefficient equal to $\alpha = 1.50$. The information on the occurrence of past events allows to define the relationship between block volume and return period, as

reported in De Biagi et al. (2017). It results that a volume of 0.2 m^3 has return period of about 10 years, while the volume corresponding to return periods of 100 and 300 years are 0.93 m^3 and 1.93 m^3, respectively. The trajectory analyses were performed using the classical rockfall softwares under lumped-mass hypothesis. The resulting empirical cumulative distributions of trajectories height and velocity at the location of the road can be described thanks to their 95th and 99th percentiles. Table 1 reports the relevant percentiles of the distribution.

To protect the road, various wall configurations were considered and their effectiveness, measured in annual failure probability (i.e., $\tau = 1$), was compared. Figure 4 sketches the problem and the main geometrical parameters. A Matlab script served to implement the formulations presented in sections 2 and 3 for the different geometrical and mechanical configurations. The analysis follows the approach already adopted by the Authors in their study on net fences (De Biagi et al. 2020, Marchelli et al. 2021, Marchelli et al. 2020). Based on the input geometry, the mechanical properties of the reinforced concrete cross-section were computed according to the simplified formulations reported in Yong et al. (2022). In a conservative approach, the energy failure calculations account for the fact that the impact occurs at the same height of the wall, i.e. the block centre of gravity of the block is at a distance from the top of the wall equal to 0.5ϕ, causing the largest effect on the system. A preliminary analysis served to qualify the parameters in the analysis and their effect on the failure probability of the system. Figure 5 reports, with the black continuous line, the annual failure probability of a 0.6 m thick wall at different design heights, from 3 to 5 m. The adopted concrete has compressive strength $f_c = 40$ MPa. The vertical rebars, having yield strength $f_y = 450$ MPa, result in a reinforcement ratio equal to 0.02. The shaded areas represent the terms p_h (in pink) and p_k (in light blue), which sum is p (the continuous line). It is seen that the failure due to excessive height (p_h) is the relevant term in the total failure probability and, as expected, this term largely reduces with taller walls. Is. Interestingly, the failure probability associated with excessive kinetic energy is higher for shorter walls rather than taller ones. This is due to several reasons: the limited mass of the wall (M) and the maximum allowable displacement (Δ_u) which is constrained by the small height of the wall, given that the plastic rotation at the base remains equal across all heights.

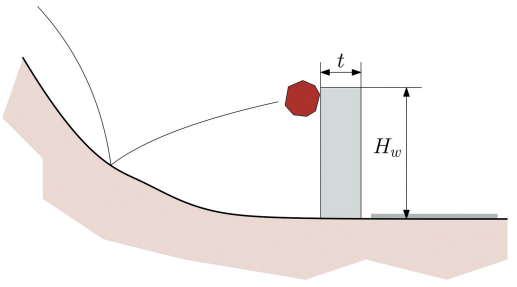


Figure 4. Sketch of the structure analysed in the example: a wall protecting a road from falling rocks.

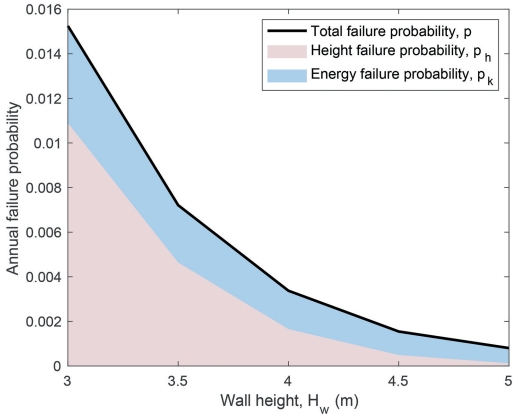


Figure 5. Failure probability for varying wall height ($t = 0.60$ m, $f_c = 40$ MPa, $q = 0.02$).

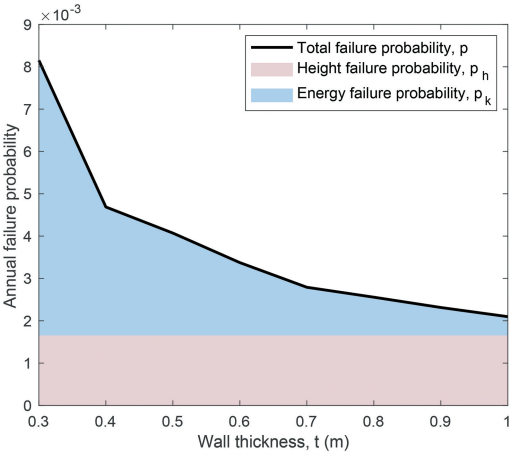


Figure 6. Failure probability for varying wall thickness ($H_w = 4$ m, $f_c = 40$ MPa, $q = 0.02$).

The second analysis referred to a wall with fixed height H_w =4 m, with varying thickness, from 0.3 to 1.0 m. The remaining properties (concrete, and reinforcement type and amount) were kept fixed as the previous example. Figure 6 plots the total annual failure probability, along with height and kinetic energy components, as in the previous example. As expected, the failure probability associated with excessive height remains constant across all thicknesses, since this failure mechanism is governed solely by the wall's height. The failure probability associated to excessive kinetic energy, on the contrary, reduces as the thickness increases, with larger reductions observed for t in the range 0.3 to 0.5 m.

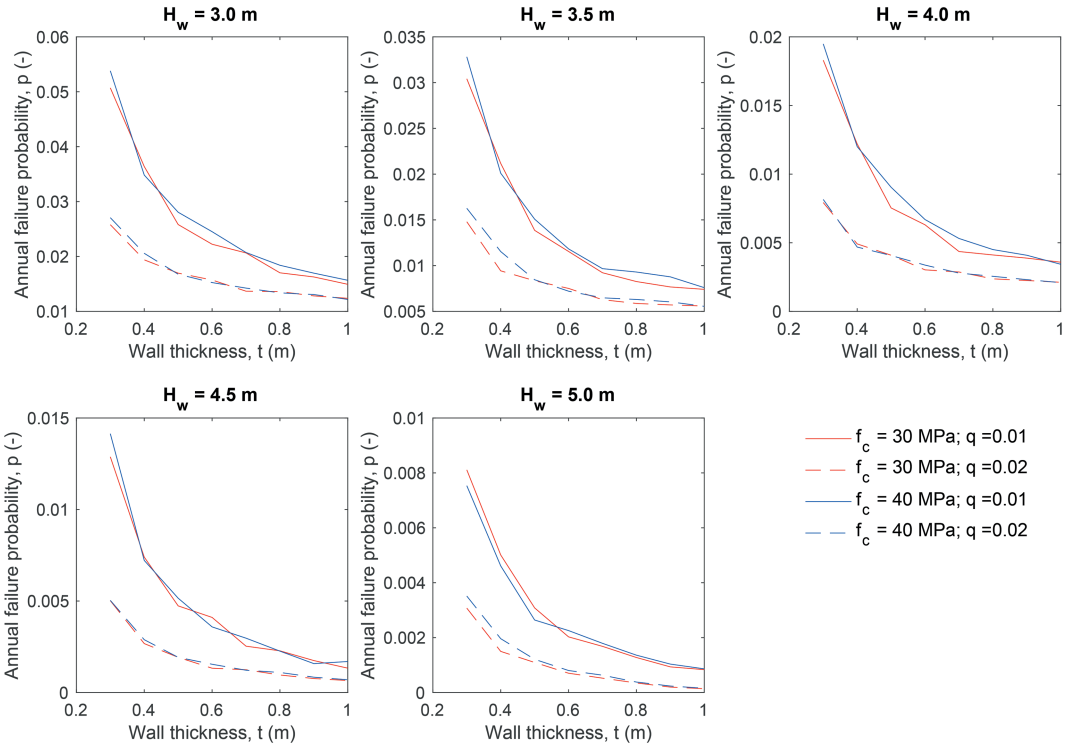


Figure 7. Annual failure probabilities for protective walls having different geometrical, material and reinforcement properties according to the parametric analysis described in the text.

This is explained by the fact that the total failure probability curve (thick continuous line) has an horizontal asymptote at the value of $p_h = 1.7 \times 10^{-3}$. Therefore, even if the wall is thickened indefinitely, the failure probability cannot be reduced below 1.7×10^{-3}. Thus, the design process involves several decisions aimed at maximizing performance by balancing the contributions of height and kinetic energy.

Finally, the parametric analysis involving different parameters was performed. The height H_w varied from 3.0 to 5.0 meters, the thicknesses t from 0.3 to 1.2 m, the vertical reinforcement ratios q either 0.01 or 0.02, and the concrete strength f_c either 30 or 40 MPa. Figure 7 reports the total annual failure probability of walls having different geometrical, material and reinforcement properties. It is observed that taller and thicker walls provide better protection, resulting in lower failure probabilities. For a given configuration of height and thickness, the most significant variation is associated with the amount of reinforcement, as indicated by continuous *vs* dashed lines. In contrast, the concrete strength, red *vs* blue, plays a very limited role in the overall performance.

In general, the selection of the most appropriate solution must satisfy target requirements in terms of failure probability. When dealing with mitigation measures protecting road infrastructure, characterised by elements at risk with non-unitary exposure, the target failure probability of the structure should not coincide with the acceptable risk along the road. Non-unitary exposure refers to situations where the elements at risk (e.g., vehicles or pedestrians) are only intermittently exposed to the hazard, such as vehicles travelling through an avalanche-prone section of a road, rather than being permanently located in the hazard zone like a building. The Authors have recently shown that the failure probability of the protective measure serves as an input to the residual risk calculation along the road, which is further moderated by traffic volume and vehicle speed (Marchelli et al. 2024).

5 CONCLUSIONS

Rockfall protection systems are essential for safeguarding infrastructure in mountainous regions where falling rocks pose significant hazards. Structural mitigation measures, such as energy-dissipating barriers, reduce impact forces by either absorbing kinetic energy through deformation or resisting impact via mass and friction. Flexible barriers (e.g., net fences) dissipate energy through large deformations but require substantial space,

limiting their use near roads. Rigid systems, such as reinforced concrete walls, overcome spatial constraints by relying on mass and bending resistance. This study presented a time-integrated reliability analysis of rigid barriers, incorporating probabilistic modelling of rockfall frequency, block size, impact velocity, and material uncertainties to address long-term reliability under variable impacts. The approach extends previous work on rockfall net fences to rigid systems. Using site-specific data, failure probabilities were evaluated over time, accounting for cumulative low-energy impacts and rare high-energy events. Results emphasise the importance of integrating temporal and probabilistic considerations into design, demonstrating that rigid barriers are effective in constrained environments but sensitive to assumptions regarding impact frequency, energy dissipation capacity, and structural degradation. It is expected that reliability-based approaches would be included in the future design practices of such structures as they are able to ensure that the mitigation measures remain effective throughout their service life.

REFERENCES

Benedikt, G. (2024). Rock falls while high-altitude mountaineering–more often in the last years? evidence from the swiss alps. *Heliyon 10*(3).

Corominas, J., N. Lantada, M. A. Núñez-Andrés, & O. C. Mavrouli (2025). Fatal non-seismic rockfalls in spain. *Geoenvironmental Disasters 12*(1), 17.

De Biagi, V., M. Marchelli, & D. Peila (2020). Reliability analysis and partial safety factors approach for rockfall protection structures. *Engineering Structures 213*, 110553.

De Biagi, V., M. L. Napoli, M. Barbero, & D. Peila (2017). Estimation of the return period of rockfall blocks according to their size. *Natural Hazards and Earth System Sciences 17*(1), 103–113.

Delonca, A., Y. Gunzburger, & T. Verdel (2014). Statistical correlation between meteorological and rockfall databases. *Natural Hazards and Earth System Sciences 14*(8), 1953–1964.

Hungr, O., S. Leroueil, & L. Picarelli (2014). The varnes classification of landslide types, an update. *Landslides 11*(2), 167–194.

Leine, R. I., A. Schweizer, M. Christen, J. Glover, P. Bartelt, & W. Gerber (2014). Simulation of rockfall trajectories with consideration of rock shape. *Multibody System Dynamics 32*(2), 241–271.

Li, L. & H. Lan (2015). Probabilistic modeling of rockfall trajectories: a review. *Bulletin of Engineering Geology and the Environment 74*(4), 1163–1176.

Maheshwari, S., R. Bhowmik, & M. Samanta (2023). Rockfall hazard: a comprehensive review of current mitigation practices. *Landslides: detection, prediction and monitoring: technological developments*, 175–209.

Marchelli, M., V. D. Biagi, & D. Peila (2020). Reliability-based design of protection net fences: influence of rockfall uncertainties through a statistical analysis. *Geosciences 10*(8), 280.

Marchelli, M., V. De Biagi, & B. Chiaia (2024). A fully probabilistic framework to compute the residual rockfall risk in presence of mitigation measures. *Landslides*, 1–8.

Marchelli, M., V. De Biagi, & D. Peila (2021). Reliability-based design of rockfall passive systems height. *International Journal of Rock Mechanics and Mining Sciences 139*, 104664.

Moos, C., Z. Bontognali, L. Dorren, M. Jaboyedoff, & D. Hantz (2022). Estimating rockfall and block volume scenarios based on a straightforward rockfall frequency model. *Engineering Geology 309*, 106828.

Yong, A. C., N. T. Lam, & S. J. Menegon (2022). *Collision actions on structures*. CRC Press.